Improved Resolution in Radio Frequency Holography: Image Spectrum Continuation and the Influence of Aberrations

E. Brundege, J. Nilles, G. Tricoles

General Dynamics Electronics Division, San Diego, CA 92186 USA

ABSTRACT

This paper describes experiment and theory on the use of imaging in radio direction finding and emitter location. Measurements were done with a 5-element array, that spanned 0.9 wavelength; the transmitter was a commercial radio station, frequnecy 1.36 MHz, at distance 10.6 km. Wavefront phase was measured with the reference signal from the central antenna; amplitude was not measured. Images were calculated by scalar diffraction theory, for ground wave propagation. Image spectra were computed. Closed form expressions for spectra were derived to guide continuation. Resolution was improved, proportional to spectrum extension. Wavefront aberrations were estimated by comparing measured and calculed phase. The effects of aberrations in continuation are discussed on relation to accuracy, resolution, and sidelobes.

INTRODUCTION

This paper describes experiment and theory on the use of imaging in radio direction finding and emitter location. Although direction finding has a long history (Gething), some interesting problems remain. Resolution is restricted by the long wavelengths and by the limited length of receiving antenna arrays. Emitter location by combining directions from separated arrays generalizes direction finding. Because the radio waves were highly coherent, speckle is considered (Goodman, 1984)

The paper describes some aspects of an image processing technique, analytic continuation, which has been studied for visible images and for microwave diffraction. (Harris), (Tricoles, et al.). The utility of continuation is questionable for noisy images; (Goodman, 1968) however, (Tricoles, et. al.) demonstrated sub-wavelength resolution by applying continuation to images with coherent speckle. Another problem may result from phase aberrations, a form of multiplicative noise in the synthesized data that are processed to form images.

The questions posed by noise and aberrations also motivated our work. The paper describes wavefront measurement, image computation, and image processing by continuation.

For the measurements the source was a commercial, amplitude modulated station that radiated at frequency 1360 kHz. Signals were received by a line array of five vertical antennas, which were spaced by 0.22 wavelength, and a phase sensitive receiver that was sequentially switched to each antenna. A reference field was derived from the central antenna; phase was recorded, but intensity was not. The phase data showed aberrations when compared to calculated values. Aberrations may have arise from adjacent buidings, fences, a buried telephone cable, or mutual coupling.

Images were calculated from the measured phase data by evaluating a fairfield, scalar diffraction integral. Ground wave propagation was assumed because the source distance was 10.6 km. Images also were calculated after reducing aberrations by replacing the measured phase value for the central antenna by the mean of the values at the two adjacent antennas. The modified wavefront was nearly linear, closely approximating the theoretical values. Images gave bearing error as $2.3^\circ \pm 0.3^\circ$ for both cases.

Spatial frequency spectra of images were theoretically analyzed. Theory was based on two assumed wavefront phase distributions; one with and one without aberrations. Closed form expressions were derived for spectra. The spectra vanish above a maximum frequency determined by array length, wavelength, and source distance. The expressions for spectra guide the analytical and numerical process of continuing spectra above the imaging system's bandpass.

Spectra were calculated for the two images from the measured and modified wavefront data. The spectra were continued. Images were then calculated by inverting the continued spectra. The images from the continued spectra had higher resolution than did the original images. Resolution improvement was potional to the spectrum extension. Bearing error was reduced to 1.5° for the image formed by continuing the spectrum of the image formed from the original measured data. Bearing error was unaffected in the other image formed by continuation.

Another effect of aberrations was on subsidiary maxima, or sidelobes. For the original measured wavefront data, continuation and inversion increased sidelobe levels above those in the image formed without continuation. For the modified data, with smaller aberrations, continuation and inversion reduced sidelobe levels below those in the image before continuation.
In summary for the cases tested, continuation processing increased resolution. Sidelobe level changes depended on aberrations. Beairng accuracy was unaffected or improved, depending on aberrations.

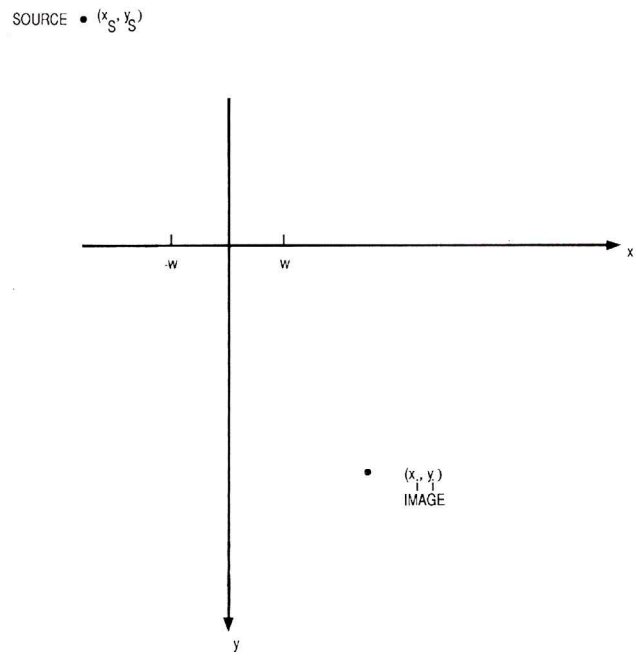

Fig. 1 - Coordinate System.

1. THEORY OF HOLOGRAPHIC IMAGING

In the co-ordinates of Figure 1, a source at (x_s , y_s) establishes a field distribution, which is measured in the interval $[-w \le t \times \le w]$ on the x-axis. To image the source, assume a lens just below the x-axis. For a monochromatic source of frequency (FORM), the complex-valued image amplitude is approximately (Baker and Copson)

$$u_i (x_i , y_i) = \int_{-w}^{w} u_h \, e^{ikp} \, e^{-i\pi x^2/\lambda f} \, dx , \qquad (1)$$

where exp $(-i\omega t)$ is suppressed, and u_h describes the measured field. A record of u_h is a hologram. The focal length of the simulated lens is f; λ is wavelength; k is $2\pi/\lambda$; i is $\sqrt{-1}$; (x_i , y_i) are iomage co-ordinates. The obliquity factor is omitted. The path length from an integration point (x,y) to an image point is

$$p = [(x_i - x)^2 + (y_i - y)^2]^{1/2} . \qquad (2)$$

With a binomial expansion,

$$p = v + (x_i - x)^2 (2v)^{-1} , \qquad (3)$$

where v replaces y_i. From Equations 1 and 3,

$$u_i (x_i , y_i) = e^{ikv} \, e^{ikx_i^2/2u} \int_{-w}^{w} u_h \, e^{-ikxx_i/u} \, dx , \qquad (4)$$

subject to the focusing condition $k/2v$ equals $\pi \lambda f$. For analysis and computation, a more convenient expression is

$$u'_i (x_i , y_i) = e^{-ikv} \, e^{-ikx_i^2/2v} \, u_i (x_i , y_i) = \int_{-w}^{w} u_h \, e^{-ikxx_i/v} \, dx . \qquad (5)$$

The properties of the data, represented by u_h, are significant. They influence quality measures such a resolution, and processing methods for image enhancement. Subsequent sections will describe measurements made with an antenna and will also describe enhancement by analytic continuation. As a preliminary, let us consider two ideal, theoretical examples, which will serve as guides for continuation.

The first example is for a single, distant source and small, receiving interval so the wave incident on the x-axis can be assumed plane. Thus,

$$u_h = e^{icx} . \qquad (6)$$

From equation 5 and 6,

$$u'_i (2w)^{-1} = sinc \, [(c - gx_i) \, w] \qquad (7)$$

where g is k/v, and sinc z is z^{-1} sinc z.

The image amplitude has largest maximum at x_i equal c/g. Resolution depends on aperture width 2w as well as k and v.

A plane incident wave is convenient for subsequent analysis but may be too idealized. In fact, measured data, described in the following section, show phase aberrations so a somewhat more realistic model is described next.

The second example models u_h by two linear phase tilts, one for each half of the aperture. That is

$$u_h = e^{ibx} \quad -w \le x < 0\,,$$

$$= e^{icx} \quad 0 < x \le w \tag{8}$$

When Equation (8) is used in Equation 5,

$$u'_i(x_i) = w^{-1} e^{-ikv} e^{-ikx_i^2/2v} u_i$$

$$= \left\{ 1 - e^{-i[b-(kx_i/v)]w} \right\} \left\{ i\,[b - (kx_i/v\,,]\,w \right\}^{-1} +$$

$$+ \left\{ e^{i\,[c-(kx_i/v)]\,w} - 1 \right\} \left\{ i\,[c - (kx_i/v)] \right\}^{-1} \tag{9}$$

The image expression in Equation 7 and 9 are utilized in the next section.

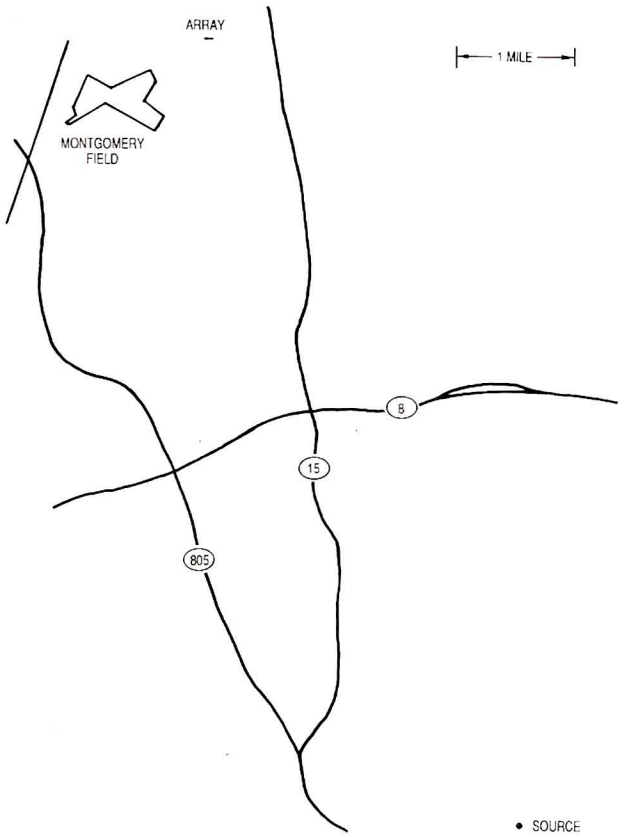

Fig. 2 - Source and Array Locations in San Diego. The numbers indicate highways:

2. MEASUREMENT

Apparatus was an antenna array, a receiver, a phase meter, and a computer controlled switch. The array included five vertical, 16-foot long antennas, spaced by 160 feet, and coaxial cables of equal length. The receiver consisted of two commercial receivers. One received a reference signal which was derived from the central antenna of the array through a power divider. Coherence was obtained by connecting the output of the reference receiver's local oscillator to the second receiver. The antennas were sequentially switched to the second receiver. The outputs of the two receivers were compared by the phase meter. The measurements obtained only phase, not amplitude; amplitude requires additional calibration.

Wavefront phase was measured for radio station KPOP which radiates amplitude modulated waves at frequency 1360 kHz, or wavelength 724 feet. Array length is thus 0.88 wavelength, and antenna spacing is 0.22 wavelength. Figure 2 shows array and source locations. The transmitter co-ordinates were x equal -2.55 milkes and y equal -6.6 miles.

Figure 3 shows measured phase values. Figure 3 also shows values calculated from path lengths to each antenna. The calculated values are plotted twice. First, a constant phase was added to all calculated values to make the calculated agree with the measured at x equal zero. Second, the calculated values were adjusted by another constant for agreement at x equal -320 feet.

Figure 3 suggests phase aberrations, specially for x = zero. Sources of error may be in the apparatus or the environment. The transmission line from the center antenna contained a power divider. In addition, the 0.22 λ antenna spacing may emphasize mutual coupling. Each antenna's phase delay was tested; values varied by only ±1° so this effect is negligible. The environment contained buildings and metallic fences. One fence had a corner approximately a half wavelengh behind the array's central antenna; the effect is unknown as a precaution a reflecting element was placed behind the array's central antenna. A buried power cable was also near the array.

Now consider the measured data in terms of the parameters b and c of the preceding section. The phase difference between the antennas at x equal - 320 feet and 0 feet is 102°; therefore, the value of b in Equation 8, for $x \le 0$ would have value 29.37 radians/mile. For $x \ge 0$ the phase

tilt is approximately zero on overage; c would have value approximately zero. If the phase value for x equal zero were ignored, the tilts on opposite sides of the origin are more nearly equal; however, the tilt for x equal -160 feet would be approximately twice that x equal 160 feet.

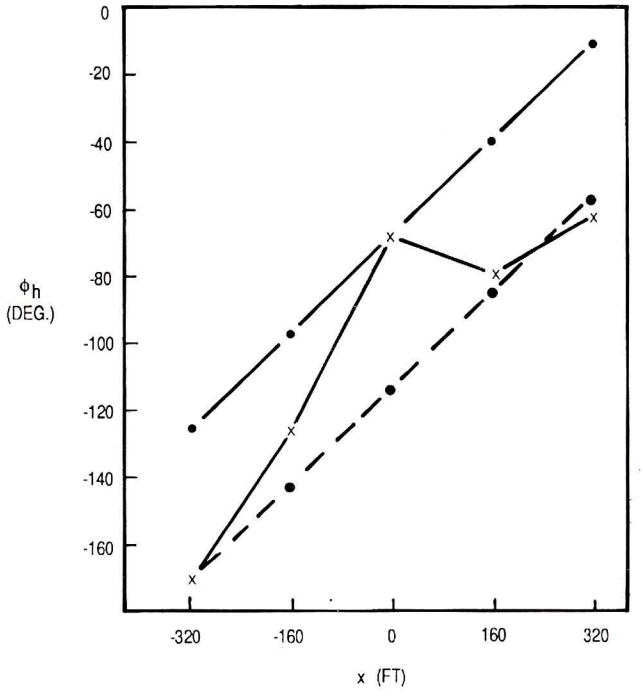

Fig. 3 - Phase measured (x) with 5 element array; frequency 1360 MHz. Calculated and adjusted to mach measured phase at x = 0, (____. ____); calculated and adjusted for agreement at x_h = -320 feet, (_ _. _ _.); The calculations were for y_h = 0; x_S = -6.6 mi; y_S = -2.55 mi. Frequency: 1360 MHz; wavelenght 724 feet.

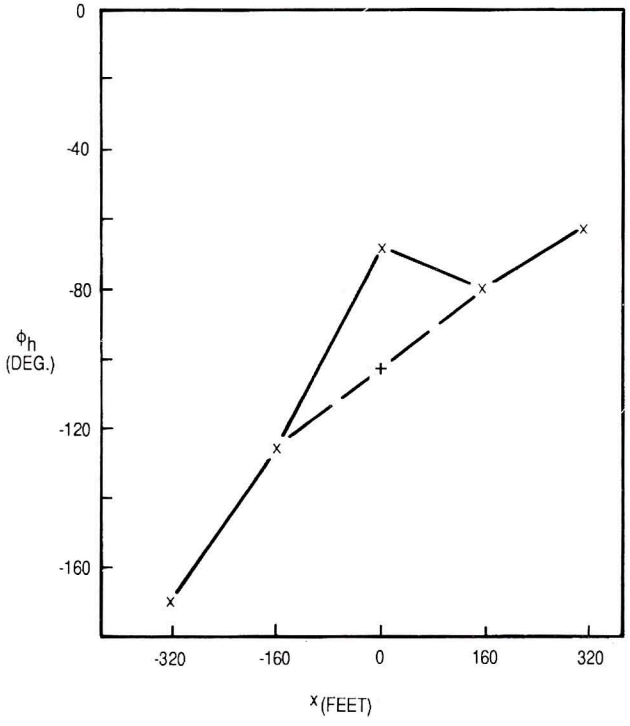

Fig. 4 - Phase values for image calculation using measured values (x); these were utilized to compute the images in Figure 5. The images in Figure 6 were based on the same data exept that for x equal zero, the value shown by (+) was used.

3. IMAGE COMPUTATION

Image were computed by evaluating equation (5) as a summation for sampled, measured data. If the data consist only of phase values Φ_m,

$$u'_i(x_i, y_i) = \sum_m e^{i\Phi_m} e^{-ikx_m x_i/v} . \qquad (10)$$

Two sets of data were utilized. The first was the measured, Figure 3. The second set differed in that the measured value at x=0 was replaced by the average of the phases at x equal ± 160 feet, locations of adjacent antennas. The graph of the second set in Figure 4 is approximately linear.

Figure 5 computed image amplitude, normalized to the peak value, for the measured phase values in Figure 3 or 4. The values are for v equal 6.6 mi.

Figure 6 shows computed values for the modified data in Figure 4; recall, modified means replacing the phase at x equal zero with the mean of the two adjacent values.

The main effect of the modification is to reduce levels of subsidiary maxima. This result is familiar in antenna theory.

4. IMAGE SPECTRA; THEORY

For the linear phase tilt, of Equation 6, the image amplitude, from Equation 7, has spectrum

$$S(\nu) = \int_{-\infty}^{\infty} u'_i e^{-2\pi\nu x_i} dx_i \qquad (11)$$

$$= e^{-i\,2\pi\nu c/g} (ig)^{-1} (I_1 - I_2) , \qquad (12)$$

where

$$I_1 = \int e^{i\tau u} u^{-1} du , \qquad (13)$$

$$I_2 = \int e^{i\sigma u} u^{-1} du , \qquad (14)$$

$$\sigma = -[1 + (2\pi\nu/gw)] , \qquad (15)$$

$$\tau = 1 - (2\pi\nu/gw) \qquad (16)$$

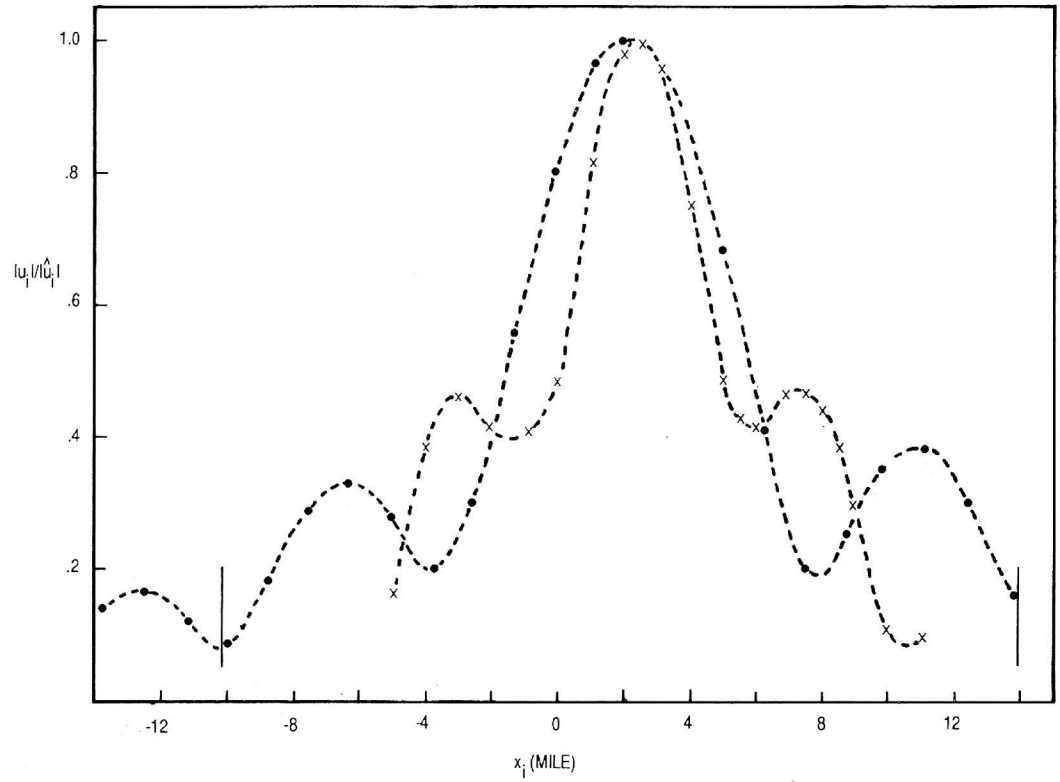

Fig. 5 - Normalized Image Amplitude. Calculated from Equation 10 with the measured phase values of Figure 4 (•). The value of v was 6.6 mi. Calculated by inverting continued spectrum (x). For (x) spectra were computed for -10 mi ≤ x ; ≤ 13.75 mi, shown by vertical bars. Images by inversion were for $|\nu| \leq 0.12$.

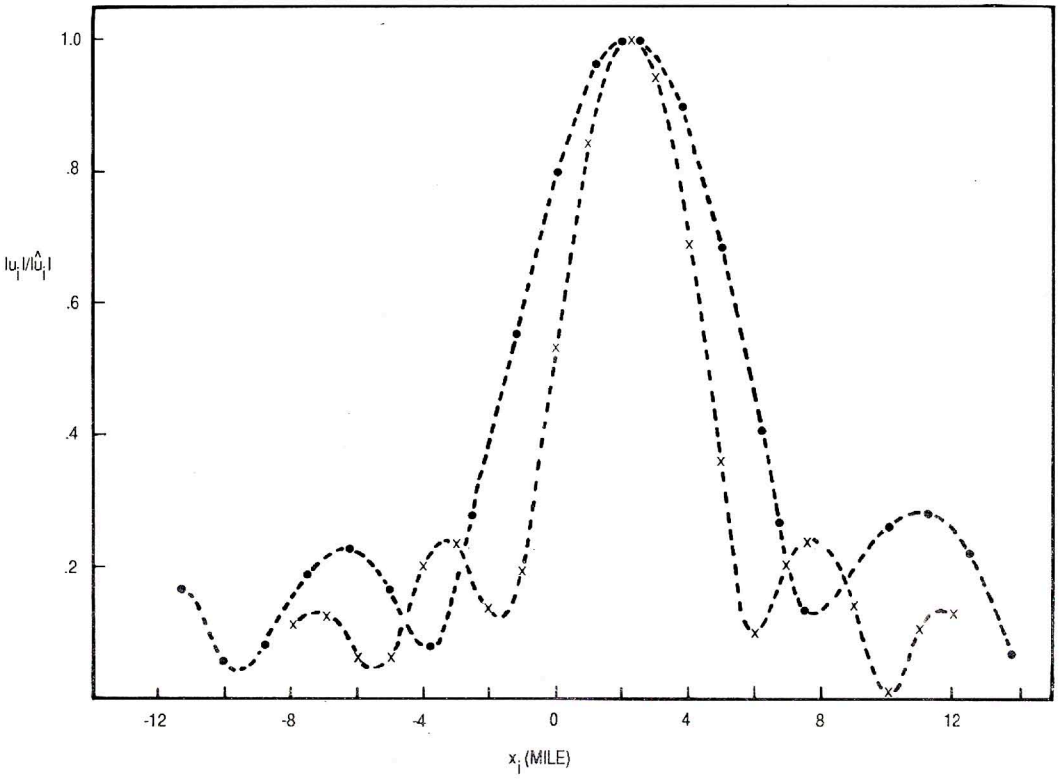

Fig. 6 - Normalized Image Amplitude. Calculated from Equation 10 with the modified phase values of Figure 4 (•). Result of continued spectrum (x) for - 10 mi $\leq x_i \leq$ *13.75 mi and* $|\nu| \leq 0.12$.

I_1 and I_2 are well known contour integrals (Smith) (Jeffreys and Jeffreys) Heaviside's unit functions. They are graphes in Figure 7, along with $I_1 - I_2$. The result is that

$$S(\nu) = \lambda v\, e^{-i\lambda c\nu\nu}, \quad |\nu| < w/\lambda v; \tag{17}$$

$$= 0, \quad |\nu| > w/\lambda v; \tag{18}$$

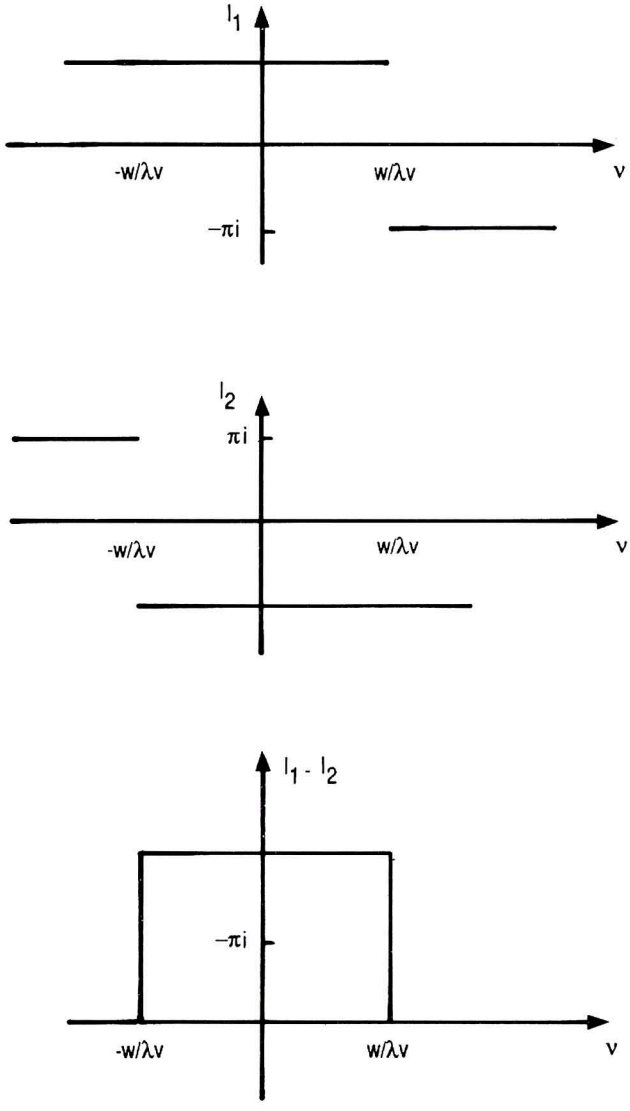

Fig. 7 - Contour Integrals $|_1$ and $|_2$

The interpretation is that object's spatial frequency spectrum is custoff at ν equal $w/\lambda v$. Recall that w is the half-width of the aperture, and 2w/v, is for small angles, the angle subtended at the object by the aperture. From the properties of Fourier transforms bigger apertures mean broader spectra, which on inversion lead to higher resolution. This result is familiar in diffraction measurements. In the above, atmospheric refraction was omitted.

For wavefront phase described by two linear tilts as in Equation 8 so that Equation 9 gives u'_i; the spectrum from equation 11 is

$$S(\nu) = I_1 - I_2 + I_3 - I_4, \tag{19}$$

where

$$I_1 = -1 \int_{-\infty}^{\infty} e^{-2\pi\nu x_i}\, b - kx_i v^{-1}\, {}^{-1}{}_{dx_i} \tag{20}$$

$$= -(\lambda v/2)\, e^{-i\lambda b\nu\nu}, \quad \nu < 0. \tag{21}$$

$$= (\lambda v/2)\, e^{-i\lambda b\nu\nu}, \quad \nu > 0. \tag{22}$$

I_4 is like I_1 except that c replaces b. For I_2 we have

$$I_2 = -i \int_{-\infty}^{\infty} e^{-i2\pi\nu x_i}\, e^{-i\,[b-(kx_i/v)]\,w}\, b - kx_i v^{-1}\, {}^{-1}{}_{dx_i} \tag{23}$$

$$= -(\lambda v/2)\, e^{-i\lambda b\nu\nu}, \quad \nu < -w/\lambda v \tag{24}$$

$$= (\lambda v/2) e^{-i\lambda b\nu\nu}, \quad \nu > w/\lambda v. \tag{25}$$

I_3 resembles I_2 except c replaces b and the step occurs at $-w/\lambda v$;

$$I_3 = -(\lambda v/2)\, e^{-i\lambda c\nu\nu}, \quad \nu < (-w/\lambda v) \tag{26}$$

$$= -(\lambda v/2)\, e^{-i\lambda c\nu\nu}, \quad \nu > (-w/\lambda v) \tag{27}$$

The meaning of equation 19 is explained by Figure 8. The range of ν is divided into four regions. For region A, $\nu < -w/\lambda v$, so from Equations 19, 21, 24, and 26, and because I_4 is like I_2 except for c replacing b,

$$S = (\lambda v/2)\left(e^{-i\lambda b\nu\nu} - e^{-i\lambda b\nu\nu} + e^{i\lambda c\nu\nu} - e^{-i\lambda c\nu\nu}\right) = 0 \tag{28}$$

For domain D $\nu > w/\lambda v$, and S is zero also. For domain B

$$S = (\lambda v/2)\left(e^{-i\lambda b\nu\nu} - e^{i\lambda b\nu\nu} - e^{-i\lambda c\nu\nu} - e^{-i\lambda c\nu\nu}\right) = -\lambda\, \nu e^{-i\lambda c\nu\nu} \tag{29}$$

Foir domain C,

$$S = \lambda \nu e^{-i\lambda b\nu\nu} \tag{30}$$

The interpretation of S when phase consists of two linear tilts is as follows. As before, the spectrum is cut off at ν equal $\pm\, w/\lambda v$ and its magnitude is constant in the interval. Phase change and hence frequency are proportional to b or c. Frequency in domain C depends on the phase slope b; similarly frequency in domain B depends on c.

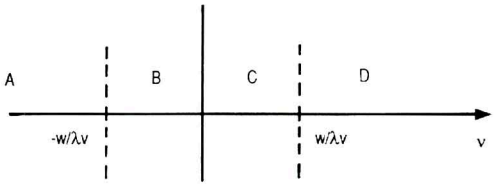

A. DOMAINS OF VARIABLE v

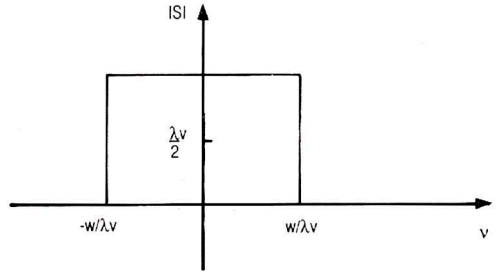

B. SPECTRUM MAGNITUDE

Fig. 8 - Definitions and | S | for phase described by two linear functions, Equation 8.

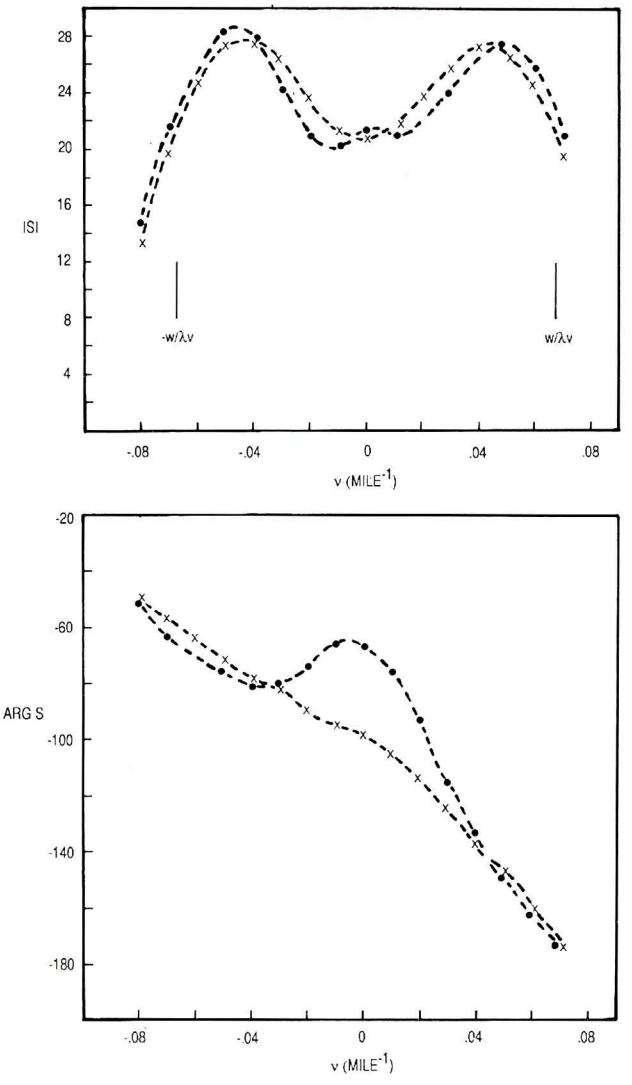

Fig. 9 - Spectra of images calculated from measured wavefront phase; - 10 mi. ≤ x_i ≤ 13.75mi . w/λ v is cutoff for w = 0.061 mi., λ = . 137mi ., v = 6.6 mi. For the image of Figure 5 (•). For the image of figure 6 (x).

5. SPECTRUM COMPUTATION

Figure 9 shows |S| and arg S for images computed from the two sets of data in Figure 4. The spectra are cut off near ± $w/\lambda v$. Magnitudes vary approximately ± 17% in the pass band. Arg S is approximately linear for the phase data modified at x_h equal zero. Arg S for the measured data is not monotonic; this is a manifestation of the phase aberration in Figure 4.

6. SPECTRUM CONTINUATION

Th spectrum S is analytic because u_i exists in a finite range and beacuse S is Fourier transform. Therefore, S can be continued beyond the cutoff given by $w\lambda v$.

The perocess of continuation assumed that the spectrum properties inside the passband exist outside. As guides for continuation, we use the closed-form, theoretical results in Equation 29 and 30. Specifically |S| is assumed constant inside and outside the passband. In addition the phase, arg S is assumed linearly proportional to n. Theoretically from equations 29 and 30, the rates of change of phase, or frequency, are – λvc and – λvb. In practice, rates are taken as those of arg S computed, in the passband, for transforms of images computed from measured wavefront phase data. For the examples two sets of data were used.

To continue the spectra, the phase was determined by inspecting arg S in Figure 9. Increments Δ (*argS*) were calculated for increments in v , Δv, and the average Δ (*argS*) was then calculated. A single value of Δv was utilized for – .06 < v < . 06. For S of the image formed from the entirely measured data, for v > 0 , Δ (*argS*) , forΔv = . 01, was - 17°, and for v < 0 Δ (*argS*) was zero. For the image formed from mod-

ified data, Figure 6 $\Delta(argS)$ was - 6°, for $\Delta\nu = .01$, for $\nu < 0$; for $\nu > 0$, $\Delta(argS)$ was - 10.2° in the same $\Delta\nu$.
Again, magnitude was assumed constant inside and outside the passband.

7. IMAGES FROM CONTINUED SPECTRA

Figure 5 shows the image computed from the continued spectrum of the image generated from the original measured wavefront phase. Figure 6 shows the image computed from the continued spectrum of the image that was generated from the modified wavefront data. In both cases, the images from continued spactra have better resolution than the originals. Continuation increased the level of subsidiary maxima in Figure 5. In contrast continuation reduced the levels of subsidiary maxima in Figure 6. Continuation reduced the bearing error for the image based on the original measured data. In this case the original image had bearing error 2.3° ± 0.3°; the continued image had bearing error 1.5° ± 0.3°. Continuation did not affect bearing error of the image based on the modified data.

CONCLUSION

This paper describes images improvement by analytic continuation of spectra of images computed from wavefront phase data that contained aberrations. Two examples were considered.

In one example, continuation improved image resolution by a factor that corresponded to the fractional bandwidth extension; in the same example, continuation increased the level of subsidiary maxima from 0.38 to 0.47 the peak value. Continuation reduced bearing error from 2.3° to 1.5°.

The second example was generated by modifying the measured wavefront data to reduce aberrations. Resolution was virtually identical to that for the aberrated data for the original and continuation images. Subsidiary maxima were reduced from 0.28 to 0.24 the peak value. Continuation did not change bearing errors.
In summary, for the examples considered, continuation improved resolution for measured phase aberrated data. Another conclusion is that aberrations raise the level of subsidiary maxima in images formed from continued spectra. Finally, bearing error reductions depended on aberrations.

REFERENCES

Gething H., *Radio Direction Finding*, Peter Peregrinus, 1978.

Goodman J., *Statistical Properties of laser Speckle*. In: Laser speckle and related phenomena, ed. by J.C. Dainty, Springer-Verlag 1984.

Harris J.L., *Diffraction and Resolving Power*, J. Opt. Soc. Am., Vol. 54, p.931 1964.

Tricoles G.; Rope L.E.; Hayward R.A., *Improved Resolution in Microwave Holographic Images* IEEE Trans, Vol. AP-29, p.320, 1981.

Goodman J.W., *Introduction to Fourier Optics*, McGraw Hill p. 133, 1968.

Baker B.B.; Copson E.T., *The Mathematical Theory of Hugyens'Principle*, Oxford 1953.

Smith L.P., *Mathematics for Engineers and Scientists*, Prentice Hall, p.174, 1956.

Jeffreys H. and Jeffreys B., *Methods of Mathematical Phyics*, Cambridge, p. 393, 1956.